Preprints of the 4th IEEE Conference on Energy Internet and Energy System Integration
October 30- November 1, 2020. Wuhan, China

Real-time Rapid Simulation Model for Faults Near the DC Drop Point Based on Dynamic Phasor Theory

Junru Shan
School of Electrical and Electronic Engineering
North China Electric Power University
Beijing, China
1003434533@qq.com

Chongru Liu
School of Electrical and Electronic Engineering
North China Electric Power University
Beijing, China
chongru.liu@ncepu.edu.cn

2020 IEEE 4th Conference on Energy Internet and Energy System Integration (EI2) | 978-1-7281-9606-0/20/$31.00 ©2020 IEEE | DOI: 10.1109/EI250167.2020.9346858

***Abstract*—In order to realize the real-time rapid calculation of faults near the DC drop point, a detailed modeling of the complete high-voltage direct-current (HVDC) system is proposed based on dynamic phasor theory. Firstly, the calculation method of actual firing angle under asymmetrical faults is analyzed, and the improved switching function model is established. Subsequently, by fully considering the dominant frequencies of harmonics and taking into account the phase shifting effect of converter transformer, the improved dynamic phasor model of converter is reconstructed to ensure the calculation accuracy at the interface between AC and DC systems. On this basis, by modeling the DC transmission line and control system, the entire HVDC system is equivalent to voltage-controlled current sources, which can output the three-phase AC fault current by only inputting three-phase AC voltage data. Applying it to the CIGRE Benchmark system, simulation results further prove the high speed and precision of the proposed model.**

Keywords—real-time rapid calculation, faults near the DC drop point, HVDC, dynamic phasor theory, voltage-controlled current source

I. INTRODUCTION

With the continuous construction of high-voltage direct-current (HVDC) transmission lines, the interconnection between AC and DC power grids has formed in China [1]. At the same time, the increase of DC drop points also has a non-negligible impact on the safety and stability of power system [2-3]. Due to the nonlinearity of the DC system, when an AC fault occurs near the DC drop point, the traditional AC fault calculation method is no longer applicable [4], so it is necessary to study this problem in detail.

The key to calculating faults near the DC drop point is to establish a proper model of the HVDC system. Currently the widely used HVDC models mainly include the electromagnetic transient (EMT) model, the quasi-steady state (QSS) model and the dynamic phasor model.

The EMT model presented in [5-7] is based on small-step simulation and detailed modeling, so its calculation accuracy is high. However, it is unsuitable for large-scale systems because of the long simulation time. Also, the EMT model requires specific modeling of the actual fault conditions, so it cannot be used to perform real-time calculation.

In contrast, the QSS model proposed by [8-9] uses linear algebraic equations to describe the electrical relationship between AC and DC systems, so the calculation time is reduced. However, traditional QSS model is based on three-phase symmetry and only considers the fundamental component [10]. So the error is extremely large when calculating asymmetrical faults. Although the QSS model proposed in [11] realizes the calculation of asymmetrical faults by considering the negative sequence component, it still cannot reflect the harmonic characteristics of the system.

On this basis, scholars have proposed the dynamic phasor model [12]. The dynamic phasor model is based on Fourier decomposition, so the balance between accuracy and simulation speed can be implemented by choosing the order of the components. In this way, it is very suitable for the rapid calculation of faults near the DC drop point. However, most of the existing dynamic phasor models are only focused on the converter part [13-15], which require external control data when simulating, so these models cannot be used to perform real-time calculations. The dynamic phasor model of the complete HVDC system is presented in [16], but it does not consider the deviation of the commutation process during an asymmetrical fault, so the error is unacceptable. Besides, none of the existing dynamic phasor models considers the influence of converter transformer, which increases the calculation error to a certain extent.

To solve this problem, this paper reconstructs a real-time rapid dynamic phasor (RTR-DP) model of the complete HVDC system for calculating faults near the DC drop point. The organization of this article is as follows. In Section II, the basic principle of dynamic phasor theory is introduced. In Section III, the calculation method of actual firing angle is discussed, and a new switching function model suitable for asymmetrical faults is proposed. Then by considering harmonics and the phase shifting effect of converter transformer, an improved dynamic phasor model of the converter is established. On this basis, Section IV finishes the modeling of DC transmission line and control system, and equates the complete HVDC system as voltage-controlled current sources. In this way, the RTR-DP model can output three-phase fault current by only inputting the three-phase voltage data. Simulation analysis under CIGRE Benchmark system is presented in Section V and Section VI summarizes the conclusions

II. BASIC PRINCIPLE OF DYNAMIC PHASOR THEORY

The dynamic phasor theory is based on Fourier decomposition. For the time domain signal $x(\tau)$, in any interval $(t\text{-}T,\ t)$, the Fourier transform and inverse transform are

This work is supported by China Southern Power Grid Technology Project. Project No: ZBKJXM20180104.

$$\begin{cases} X_k(t)=\dfrac{1}{T}\int_{t-T}^{t} x(\tau)e^{-jk\omega\tau}d\tau \\ x(\tau)=\sum_{k=-\infty}^{\infty} X_k(t)e^{jk\omega\tau} \end{cases} \tag{1}$$

Where $\omega=2\pi/T$. $X_k(t)$ is the kth Fourier coefficient and also the kth dynamic phasor of the time domain signal. $X_k(t)$ can be written as $\langle x\rangle_k$. Dynamic phasors have the following conjugate, product and differential characteristics:

$$\begin{cases} \langle x\rangle_{-k}=\langle x\rangle_k^* \\ \langle xy\rangle_k=\sum_i \langle x\rangle_{k-i}\cdot\langle y\rangle_i \\ \left\langle \dfrac{dx}{dt}\right\rangle_k=\dfrac{d}{dt}\langle x\rangle_k+jk\omega\langle x\rangle_k \end{cases} \tag{2}$$

Where superscript * represents the conjugate of the phasor.

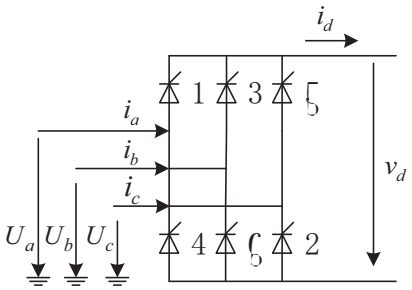

Fig. 1. Six-pulse converter

On this basis, according to the modulation theory, the electrical relationships between AC and DC sides of the six-pulse converter shown in Fig. 1 can be expressed as

$$\begin{cases} v_d=U_aS_{va}+U_bS_{vb}+U_cS_{vc} \\ i_a=i_dS_{ia} \\ i_b=i_dS_{ib} \\ i_c=i_dS_{ic} \end{cases} \tag{3}$$

Where v_d and i_d are the direct voltage and direct current of the converter. U_a, U_b, U_c and i_a, i_b, i_c are the three-phase voltage and current of the ac side of the converter. S_{va}, S_{vb}, S_{vc} and S_{ia}, S_{ib}, S_{ic} represent the three-phase switching functions for voltage and current. According to (2) and (3), the dynamic phasor model of the converter is

$$\langle v_d\rangle_k=\sum_i\sum_{m=a,b,c}\langle U_m\rangle_{k-i}\langle S_{vm}\rangle_i \tag{4}$$

$$\langle i_m\rangle_k=\sum_i\langle i_d\rangle_{k-i}\langle S_{im}\rangle_i \tag{5}$$

Where m=a, b, c represents phase a, phase b and phase c. The dynamic phasor model of the converter can be simplified by ignoring the high-frequency components as needed.

III. Improved Dynamic Phasor Model of Converter

A. Calculation Method of Actual Firing Angle

When an asymmetrical fault occurs near the DC drop point, the asymmetry of the commutation voltage will cause the actual firing angle to change. At present, most HVDC projects use the equal interval firing mode. In this mode, control system sends firing pulses to each valve based on the synchronous phase output by the phase-locked loop (PLL).

The basic working principle of the PLL is to decompose the three-phase commutation voltage into α,β components and input the components to the proportional-integral (PI) controllers. Then the PLL can output the initial phase of the synchronous voltage, that is

$$\varphi_{PLL}=\arctan\left(\frac{U_\alpha\sin\varphi_\alpha+U_\beta\cos\varphi_\beta}{U_\alpha\cos\varphi_\alpha-U_\beta\sin\varphi_\beta}\right) \tag{6}$$

Where U_α, U_β and φ_a, φ_β are the amplitude and initial phase of the α, β component of the commutation voltage.

When the HVDC system is running normally, φ_{PLL} is also the initial phase of the commutation voltage U_{ac}. As shown in Fig. 2(a), U_{PLL} represents the synchronous voltage with initial phase φ_{PLL}, α is the firing angle order, U_{ac}, U_{ba}, U_{cb} are the actual commutation voltage. The control system sends pulse P_1 to valve 1 after delaying α from the zero crossing of U_{PLL}, and then sends pulse P_n (n=2,3,...,6) to the remaining valves in turn after a delay of $\pi/3$.

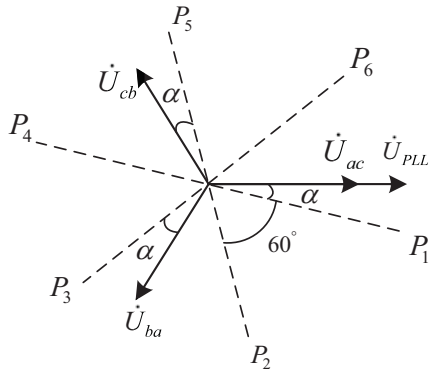

(a) Symmetrical condition

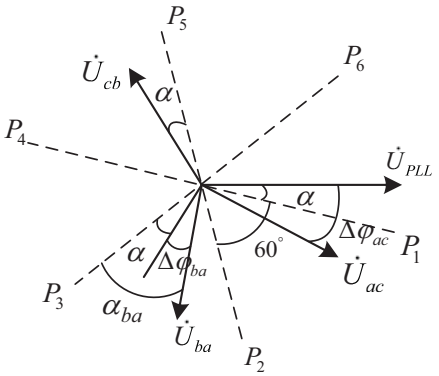

(b) Asymmetrical condition

Fig. 2. Deviation of the commutation voltage under different conditions

But when there is an asymmetrical fault near the DC drop point, due to the asymmetry of the three-phase voltage, φ_{PLL} is not the initial phase of U_{ac} anymore. However, the control system still sends pulses based on φ_{PLL}, so when the pulse arrives, the converter valve may cannot be turned on due to the negative commutation voltage.

Fig. 2(b) shows the deviation of the actual commutation voltage when a-phase near the DC drop point is grounded. For the commutation process from c-phase to a-phase, it can be seen from the figure that the actual commutation voltage

U_{ac} and the synchronous voltage U_{PLL} have a phase deviation, that is, $\Delta\varphi_{ac}=\varphi_{PLL}-\varphi_{ac}$, where φ_{ac} is the initial phase of U_{ac}. At this time, $\Delta\varphi_{ac}>\alpha$, so the commutation voltage U_{ac} is still negative when the pulse P_1 arrives. This means valve 1 cannot be turned on for now. Valve 1 will be turned on immediately after U_{ac} changes from negative to positive. Therefore, the actual firing angle $\alpha_{ac}=0$.

As for the commutation process from a-phase to b-phase, the phase deviation is $\Delta\varphi_{ba}=\varphi_{PLL}-2\pi/3-\varphi_{ba}$, where φ_{ba} is the initial phase of U_{ba}. Fig. 2(b) shows that $\Delta\varphi_{ba}<0<\alpha$, so the commutation voltage U_{ba} is already positive when the pulse P_3 arrives. Valve 3 can be turned on normally. Therefore, the actual firing angle $\alpha_{ba}=\alpha-\Delta\varphi_{ba}$. In summary, the actual firing angle for the commutation process from n-phase to m-phase can be calculated as (7)

$$\alpha_{mn}=\begin{cases}0 & \Delta\varphi_{mn}\geq\alpha\\ \alpha-\Delta\varphi_{mn} & \Delta\varphi_{mn}<\alpha\end{cases} \tag{7}$$

Apparently, the deviation $\Delta\varphi_{mn}$ is equal to zero when three phases of AC system are symmetrical, and the actual firing angle α_{mn} is equal to the angle order α in this case.

B. Improved Switching Function Model

After calculating the actual firing angle, the actual commutation angel needs to be recalculated as follows:

$$\mu_{mn}=\arccos\left(\cos\alpha_{mn}-\frac{\sqrt{2}X_r i_d}{E_{mn}}\right)-\alpha_{mn} \tag{8}$$

Where E_{mn} is the effective value of the commutation voltage; X_r is the commutation reactance.

In cases of asymmetrical faults, each commutation process is no longer symmetrical, so the switching function needs to configure the firing angle and commutation angle independently for each commutation process. Therefore, this paper decomposes the switching function into four components: the basic component S_n, the delay component S_m, the commutation component $S_{u\mu}$ of the voltage switching function, and the commutation component $S_{i\mu}$ of the current switching function. The components are shown in Fig. 3

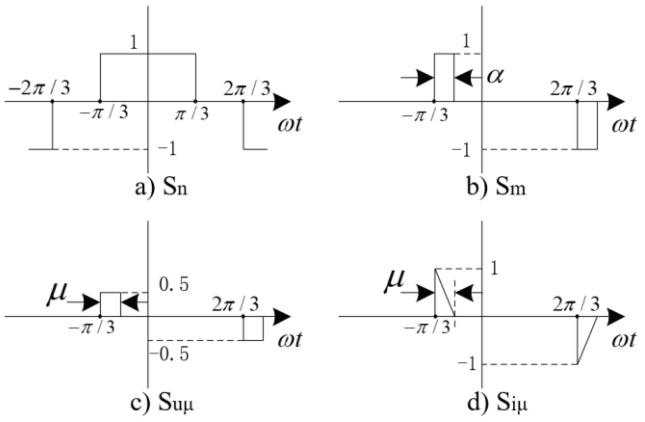

Fig. 3. Components of switching functions

According to the coordinate system shown in Fig. 3, the components are decomposed into Fourier series, and the kth Fourier coefficients of each component are

$$\begin{cases}S_n(k)=\dfrac{e^{jk\pi/3}}{2\pi k}\left[\left(\sin\dfrac{2k\pi}{3}-\sin\dfrac{5k\pi}{3}\right)+\right.\\ \qquad\left.j\left(\cos k\pi+\cos\dfrac{2k\pi}{3}-\cos\dfrac{5k\pi}{3}-1\right)\right]\\ S_m(k,\alpha)=\dfrac{e^{jk\pi/3}}{2\pi k}\left[\left(\sin(k\alpha)-\sin(k\pi+k\alpha)\right)+\right.\\ \qquad\left.j\left(\cos(k\pi)+\cos(k\alpha)-1-\cos(k\pi+k\alpha)\right)\right]\\ S_{u\mu}(k,\mu)=\dfrac{e^{jk\pi/3}}{4\pi k}\left[\left(\sin(k\mu)-\sin(k\pi+k\mu)\right)+\right.\\ \qquad\left.j\left(\cos(k\pi)+\cos(k\mu)-1-\cos(k\pi+k\mu)\right)\right]\\ S_{i\mu}(k,\mu)=\dfrac{e^{jk\pi/3}}{2\pi k^2\mu}\left[(1-jk\mu)\left(1-e^{-jk\pi}\right)-\right.\\ \qquad\left.e^{-jk\mu}+e^{-jk(\pi+\mu)}\right]\end{cases} \tag{9}$$

For the a-phase switching function, it includes two commutation processes: the commutation process from c-phase to a-phase and from a-phase to b-phase. So the kth dynamic phasors of each component are

$$\begin{cases}\langle S_{na}\rangle_k=S_n(k)\\ \langle S_{ma}\rangle_k=S_m(k,\alpha_{ba})e^{-jk\frac{2\pi}{3}}-S_m(k,\alpha_{ac})\\ \langle S_{u\mu a}\rangle_k=S_{u\mu}(k,\mu_{ba})e^{-jk\left(\frac{2\pi}{3}+\alpha_{ba}\right)}-\\ \qquad S_{u\mu}(k,\mu_{ac})e^{-jk\alpha_{ac}}\\ \langle S_{i\mu a}\rangle_k=S_{i\mu}(k,\mu_{ba})e^{-jk\left(\frac{2\pi}{3}+\alpha_{ba}\right)}-\\ \qquad S_{i\mu}(k,\mu_{ac})e^{-jk\alpha_{ac}}\end{cases} \tag{10}$$

Therefore, the kth dynamic phasors of the a-phase switching function can be obtained by superimposing the corresponding components, as shown in (11)

$$\begin{cases}\langle S_{va}\rangle_k=\langle S_{na}\rangle_k+\langle S_{ma}\rangle_k+\langle S_{u\mu a}\rangle_k\\ \langle S_{ia}\rangle_k=\langle S_{na}\rangle_k+\langle S_{ma}\rangle_k+\langle S_{i\mu a}\rangle_k\end{cases} \tag{11}$$

Where S_{va} represents the a-phase switching function for voltage, and S_{ia} represents the a-phase switching function for current.

The calculation principles of the b-phase and c-phase switching functions are the same as above, except that the commutation process they contain are different, and the phase of their kth dynamic phasor lags and leads the a-phase switching function by $2\pi k/3$, respectively.

C. Improved Dynamic Phasor Model of Converter Considering Harmonics

It can be concluded from [15] that in order to ensure the calculation accuracy, 0th and 2nd dynamic phasors must be considered on the DC side of the converter, and 1st and 3rd dynamic phasors must be considered on the AC side. So the calculation speed can be improved by ignoring other high frequency components. According to (4), the dynamic phasor of the DC voltage can be calculated as (12)

$$\begin{cases} \langle v_d \rangle_0 = \sum\limits_{m=a,b,c} \langle U_m \rangle_1 \langle S_{vm} \rangle_1^* + \sum\limits_{m=a,b,c} \langle U_m \rangle_1^* \langle S_{vm} \rangle_1 \\ \langle v_d \rangle_2 = \sum\limits_{m=a,b,c} \langle U_m \rangle_1 \langle S_{vm} \rangle_1 + \sum\limits_{m=a,b,c} \langle U_m \rangle_1^* \langle S_{vm} \rangle_3 + \\ \qquad \sum\limits_{m=a,b,c} \langle U_m \rangle_3 \langle S_{vm} \rangle_1^* + \sum\limits_{m=a,b,c} \langle U_m \rangle_3^* \langle S_{vm} \rangle_5 \end{cases} \quad (12)$$

Similarly, according to (5), the dynamic phasor of the three-phase AC current is

$$\begin{cases} \langle i_m \rangle_1 = \langle i_d \rangle_0 \langle S_{im} \rangle_1 + \langle i_d \rangle_2 \langle S_{im} \rangle_1^* + \langle i_d \rangle_2^* \langle S_{im} \rangle_3 \\ \langle i_m \rangle_3 = \langle i_d \rangle_0 \langle S_{im} \rangle_3 + \langle i_d \rangle_2 \langle S_{im} \rangle_1 + \langle i_d \rangle_2^* \langle S_{im} \rangle_5 \end{cases} \quad (13)$$

Thus, according to (1), the time domain value of the DC voltage and AC current can be calculated by (14)

$$\begin{cases} v_d(t) = \langle v_d \rangle_0 + 2\,\mathrm{Re}\left(\langle v_d \rangle_2 e^{j2\omega t} \right) \\ i_m(t) = 2\,\mathrm{Re}\left(\langle i_m \rangle_1 e^{j\omega t} + \langle i_m \rangle_3 e^{j3\omega t} \right) \end{cases} \quad (14)$$

D. Influence of Converter Transformer on the Improved Dynamic Phasor Model of Converter

Normally, two 6-pulse bridges are connected in what is called a 12-pulse configuration by using Y-Y and Y-D transformers. For the Y-D converter transformer shown in Fig. 4, there is a phase shifting effect between the converter side and the AC bus side.

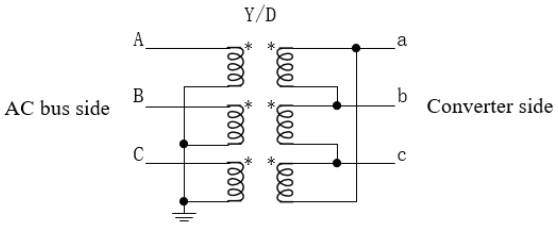

Fig. 4. Model of Y-D transformer

Assuming the ratio of the converter transformer is K, so we have

$$\begin{cases} U_{ba} = -KU_A \\ U_{cb} = -KU_B \\ U_{ac} = -KU_C \end{cases} \quad (15)$$

It can be known from the working principle of converter that the three-phase voltage switching functions satisfy:

$$S_{va} + S_{vb} + S_{vc} = 0 \quad (16)$$

Therefore, in combination with (3), the DC voltage of the Y-D connected bridge should be rewritten as

$$\begin{aligned} v_d &= U_a S_{va} + U_b S_{vb} + U_c S_{vc} \\ &= U_a S_{va} + U_b S_{vb} + U_c \left(-S_{va} - S_{vb} \right) \\ &= \left(U_a - U_c \right) S_{va} + \left(U_b - U_c \right) S_{vb} \\ &= U_{ac} S_{va} - U_{cb} S_{vb} \end{aligned} \quad (17)$$

The dynamic phasor equivalent of (17) can be obtained according to (2) with k=0 and 2 (to denote 0th and 2nd dynamic phasors).

IV. Modeling of the Complete HVDC System

A. DC Transmission Line

As shown in Fig. 5, the DC transmission line can be equivalent to the T-type model, where L_d, R_d and C_d represent the inductance, resistance and capacitance of DC transmission line, respectively.

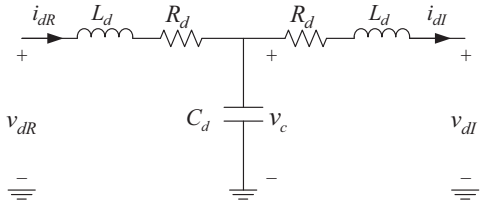

Fig. 5. T-type model of DC transmission line

The letter "R" in the subscript represents the rectifier side, and "I" represents the inverter side (the same below). The differential equations for DC transmission line are

$$\begin{cases} L_d \dfrac{di_{dR}}{dt} = v_{dR} - v_c - R_d i_{dR} \\ L_d \dfrac{di_{dI}}{dt} = v_c - v_{dI} - R_d i_{dI} \\ C_d \dfrac{dv_c}{dt} = i_{dR} - i_{dI} \end{cases} \quad (18)$$

The dynamic phasor equivalent of (18) can be obtained according to (2) with k=0 and 2. Then it can be used to calculate the dynamic phasor of DC current.

B. HVDC Control System

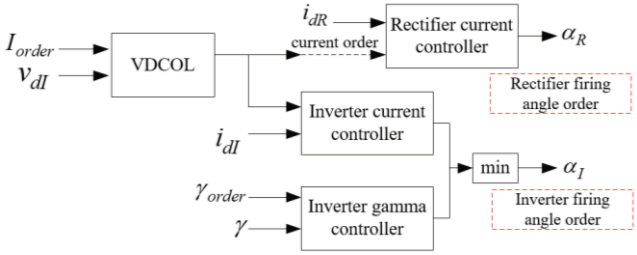

Fig. 6. HVDC control system

Fig. 6 shows the diagram of HVDC control system. Normally, the rectifier side operates in constant current control mode, and the inverter side operates in constant extinction-angle(γ) control mode. The output of control system is the firing angle order that can be used in Section III.

On this basis, differential equations are established according to the controller parameters provided by the CIGRE Benchmark system, and the firing angle order is obtained by using the numerical integration method. The main controller gains and time constants are listed in Table I.

TABLE I. Controller Parameters

Controller	Parameter	Rectifier	Inverter
Current controller	Proportional gain	1.0989	0.63
	Integral time constant	0.01092	0.01524
Gamma controller	Proportional gain	-	0.7506
	Integral time constant	-	0.0544

C. Equivalent Model of the Complete HVDC System

It is pointed out in [17] that when various types of faults occur near the DC drop point, the change of three-phase voltage at the fault point is consistent with that in the pure AC system. Therefore, the key to studying fault characteristics is to calculate the three-phase fault current.

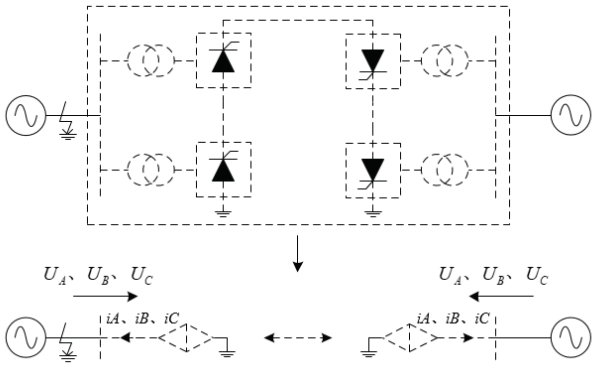

Fig. 7. Voltage-controlled current source model of HVDC system

After modeling the HVDC converter, DC transmission line and HVDC control system, the entire HVDC system including converter transformer can be equivalent to voltage-controlled current sources. In this way, as long as three-phase AC voltage data is input, the equivalent model can output equal-length three-phase AC current data in real time. The equivalent process is shown in Fig. 7.

Based on the above analysis, the proposed RTR-DP model can already perform real-time rapid calculation of faults near the DC drop point. The flow chart is shown in Fig.8.

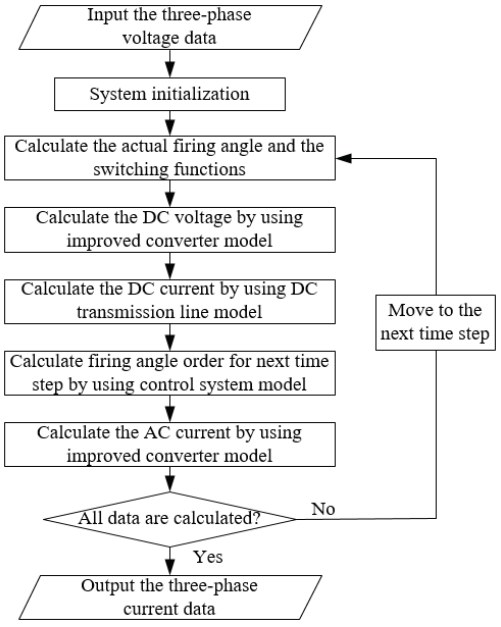

Fig. 8. Calculation flow chart

V. Simulation Results and Model Verification

The proposed RTR-DP model is programmed in MATLAB based on the CIGRE Benchmark system. Then, in order to verify its effectiveness, the simulation results of the RTR-DP model and the EMT model in PSCAD are compared under various scenarios shown in Table II.

TABLE II. Description of Simulation Scenarios

Cases	Description
Case 1	a-phase near the rectifier side is grounded at 2.0s and lasts 0.1s
Case 2	a-phase near the rectifier side is grounded at 2.0s and lasts 0.2s, and b-phase is grounded at 2.04s and lasts 0.15s
Case 3	Three-phase near the rectifier side are grounded at 2.0s and lasts 0.1s

In order to prevent commutation failure, all faults are on the rectifier side. The simulations shown in this paper are conducted with a time step of 100μs for both the EMT and RTR-DP model, and the system cycle T=0.02s. The comparison of three-phase fault current on the rectifier side is shown in Fig. 9.

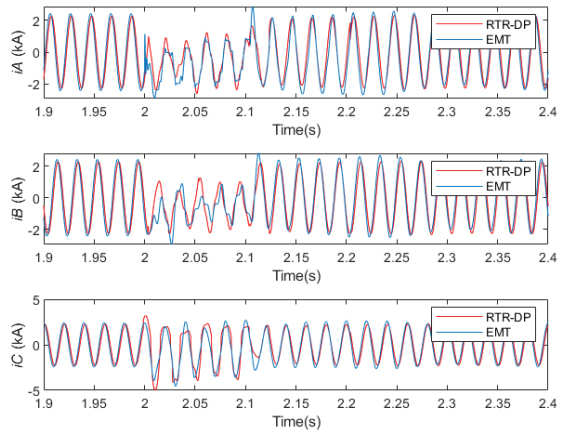

(a) Case 1

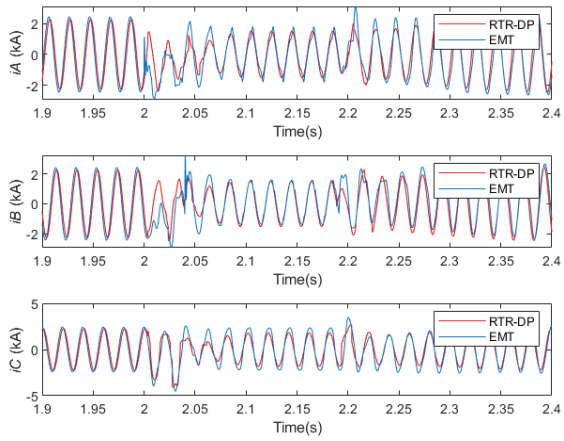

(b) Case 2

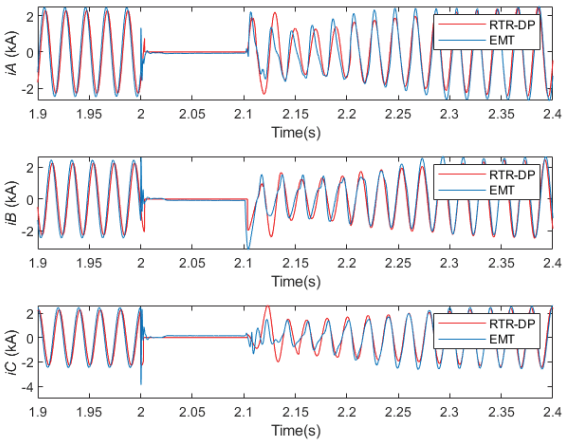

(c) Case 3

Fig. 9. Simulation results of three-phase fault current

The traces in Fig. 9 show conformity between results of the RTR-DP model and the EMT model, which means the proposed model can follow the system response well under both symmetrical and asymmetrical faults. In addition, due to the accurate modeling of the complete HVDC system, the proposed RTR-DP model can also output the DC voltage and current in the real-time simulation if needed.

To further prove the high speed and precision of the RTR-DP simulation model, the time-consuming coefficient and residual similarity are used to analyze the simulation results. The time-consuming coefficient is defined as

$$\sigma = \frac{t_{DP}}{t_{EMT}} \tag{19}$$

Where t_{DP} and t_{EMT} are the calculation time of the proposed RTR-DP model and EMT model. The calculation of residual similarity is

$$\begin{aligned} \gamma_i &= \frac{|y_i|}{\sum_{i=1}^{N}|y_i|} \\ x_i &= 1-\frac{|y_i - z_i|}{\max\left(|y_i|,|z_i|\right)} \\ \varphi &= \sum_{i=1}^{N}\gamma_i x_i \end{aligned} \tag{20}$$

where y and z are the EMT and RTR-DP results, respectively. φ is the residual similarity.

TABLE III. ANALYSIS OF SIMULATION PERFORMANCE

Cases	Time-consuming coefficient	Residual similarity		
		iA	*iB*	*iC*
Case 1	0.92	92.3%	91.1%	90.5%
Case 2	0.87	91.4%	90.2%	90.8%
Case 3	0.88	93.4%	93.0%	92.5%

As shown in Table III, the time-consuming coefficient is less than one in each case, which means the RTR-DP model can perform faster calculation than the EMT model. On the other hand, it is generally believed that when the residual similarity is greater than 80%, the simulation model can meet the error requirements [18]. Since the residual similarity in each case is greater than 90%, the RTR-DP simulation model has high accuracy for faults near the DC drop point.

VI. CONCLUSIONS

This paper reconstructs the simulation model of the complete HVDC system based on dynamic phasor theory, and the validity of the model is proved by simulations under the CIGRE Benchmark system. The following conclusions can be made after performing above analysis:

1) The proposed RTR-DP model can perform faster calculation than the EMT model, so it provides the possibility of rapid simulation for large-scale systems.

2) Through the calculation of the actual firing angle and modeling of the improved switching functions, the proposed RTR-DP model can perform accurate simulation under various asymmetrical faults near the DC drop point.

3) By modeling the complete HVDC system as voltage-controlled current sources, the RTR-DP model can easily select corresponding input of voltage according to different tasks to realize the extended application. For example, if the input is real-time AC bus voltage of the converter station, this model can realize rapid tracking of the DC system response and checking of the system status; The input can also be the predicted fault voltage of the AC system, so the model can achieve rapid assessment of the system safety margin and early warning of the hypothetical faults.

REFERENCES

[1] X. M. Liang, P. Zhang and Y. Chang, "Recent advances in high-voltage direct-current power transmission and its developing potential," Power System Technology, 2012,36(4): 1-9.

[2] M. J. Li, "Characteristic analysis and operational control of large-scale hybrid UHV AC/DC power grids," Power System Technology, 2016,40(4):985-991.

[3] Y. Tang, Q. Guo, Q. Y. Zhou, Q. Qin and X. H. Qin, "Security evaluation for UHV synchronized power grid," Power System Technology, 2016,40(1): 97-104.

[4] C. H. Ma, W. C. Zhang, Q. Xu and S. Q. Yang, "AC/DC power system fault simulation based on ADPSS," 4th International Conference on Electric Utility Deregulation and Restructuring and Power Technologies (DRPT), 2011: 514-518.

[5] X. X. Zhou, F. Tian, Y. L. Li and C Zheng, "Parallel computing and digital simulation of power system," Beijing: Tsinghua University Press, 2014:185-187.

[6] N. Watson and J. Arrillaga, "Power systems electromagnetic transient simulation," London: The Institution of Engineering and Technology, 2007: 92-95.

[7] Y. F. Liang, X. Lin, Ani M. Gole and M. Yu, "Improved coherency-based wide-band equivalents for real-time digital simulators," IEEE Transactions on Power Systems, 2010, 26(3): 1410-1417.

[8] C. Osauskas and A. Wood, "Small-signal dynamic modeling of HVDC systems," IEEE Transactions on Power Delivery, 2003, 18(1): 220-225.

[9] C. C. Zhou and Z. Xu, "Simulation validity test of the HVDC Quasi-Steady-State model," Proceedings of the CSEE, 2003(12): 36-39.

[10] X. M. Mao, Y. Zhang and Y. Zhang, "Survey on HVDC modeling," Electric Power Automation Equipment, 2007, 12(27): 14-27.

[11] J. Y. Huang, L. Wang and Z. Z. Qi, "A new transient stability program for AC-DC interconnection system," Proceedings of the CSEE, 1988(06): 3-10.

[12] Q. R. Qi, L. W. Jiao, Z. Yan, Y. X. Ni and S. S. Chen, "Modeling and simulation of HVDC with dynamic phasors," Proceedings of the CSEE, 2003, 23(12): 28-32.

[13] W. B. Luo and G. L. Zhao, "Modeling and simulation of asymmetrical faults in HVDC," China Electric Power (Technology Edition), 2013(7): 28-32.

[14] M. Daryabak, S. Filizadeh, J. Jatskevich, et al., "Modeling of LCC-HVDC system using dynamic phasors," IEEE Transactions on Power Delivery, 2014, 29(4): 1989-1998.

[15] S. Y. Zeng, Q. Y. Jiang, S. Q. Lu, M. Zhao and X. W. Xu, "Dynamic phasors model of line commutated converter under unbalanced conditions," Automation of Electric Power Systems, 2018, 42(11): 129-135+150.

[16] Y. H. Zhao, C. R. Liu, G. Y. Li and F. L. Yun, "Modeling and simulation of HVDC systems by three-phase dynamic phasor," Journal of System Simulation, 2017, 29(04): 752-760.

[17] Y. C. Zhu, "Characteristics of the fault near converter station and its influence on security and stability control devices," North China Electric Power University, 2015.

[18] X. D. Jia, G. Y. Li, C. Y. Zhao, X. N. Xiao, W. Q. Han and Q. Guo, "Study of the credibility evaluation method for the power system simulation," Proceedings of the CSEE, 2010, 30(19): 51-57.